ACS SENSORS

pubs.acs.org/acssensors

Article

Ultrasensitive Detection of Nitrite through Implementation of *N*-(1-Naphthyl)ethylenediamine-Grafted Cellulose into a Paper-Based Device

Teresa L. Mako, Adelaide M. Levenson, and Mindy Levine*

Cite This: *ACS Sens.* 2020, 5, 1207−1215

Read Online

ACCESS | Metrics & More | Article Recommendations | Supporting Information

ABSTRACT: Reported herein is the immobilization of *N*-(1-naphthyl)ethylenediamine (NED) on cellulose via an epichlorohydrin (ECH)-based covalent attachment and the implementation of the functionalized cellulose into an ultrasensitive, paper-based device for nitrite detection. The reported functionalization procedure resulted in a 12.9-fold higher functionalization density than the density that results from the previously reported procedures, and the subsequent device allows for nitrite detection limits in synthetic freshwater and real seawater of 0.26 and 0.22 μM, respectively. The sensor is efficient in a wide range of temperature, humidity, turbidity, and salinity conditions and has been successfully applied for nitrite detection in real water samples.

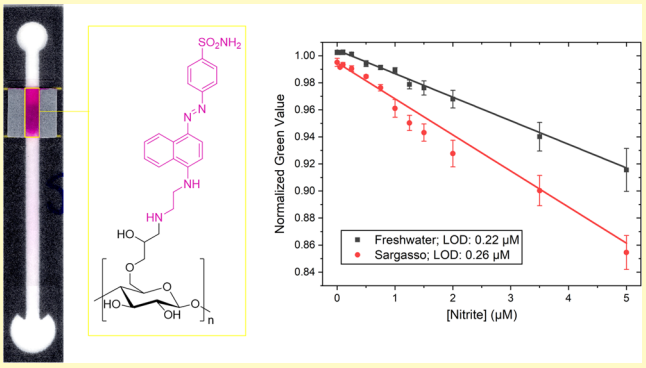

KEYWORDS: *paper-based device, nitrite, colorimetric detection, cellulose modification, Griess reaction*

Nitrite, a prevalent environmental contaminant[1−4] that is released into the environment by human activities such as wastewater treatment, agricultural activities, and industrial processes,[5−7] can successfully be quantified at sub-micromolar levels using techniques such as capillary electrophoresis, spectrophotometry, electrochemical detection, and ion chromatography.[8,9] While these techniques are useful in laboratory settings, in most cases, they are not easily translocated for onsite, real-time measurements, despite the need to detect nitrite in the field. Many commercially available dipstick test strips have been designed for onsite use, yet these cannot detect sub-micromolar levels that are relevant for environmental monitoring.

Attractive alternatives to both instrumental techniques and dipstick test strips are paper-based devices.[10,11] Paper-based devices often rely on precisely patterned hydrophilic channels through which the sample solutions flow, facilitated by capillary action and controlled using hydrophobic barriers. Sequentially timed delivery of reagents, and thus multistep processes, can be mediated by this controlled flow.[12] These channels can be utilized to eliminate sample pretreatments, such as purification, concentration, dilution, or reagent addition, that are often required prior to instrumentation-based techniques. Additional benefits of paper-based devices include that they require only microliter quantities of sample, as opposed to milliliter volumes required for instrumentation-based quantification,[12] and often can be analyzed by naked-eye detection, smartphones,[13,14] or flatbed scanners.[15−18] Based on these known advantages of paper-based devices and the continued need for improved sensors for onsite nitrite detection, we aimed to construct a nitrite-sensitive paper-based device that improves upon the limitations of known techniques and enables highly sensitive, robust, and practical onsite detection.

Most commercially available test strips rely on the inexpensive and user-friendly Griess method,[19−21] a colorimetric technique that allows simple naked-eye quantitation through comparison on a color scale. The Griess reaction typically utilizes two indicators, sulfanilamide and *N*-(1-naphthyl)ethylenediamine (NED), which, in the presence of nitrite, form a highly colored azo dye (Scheme 1).[14] Sulfanilamide first reacts with nitrite to form a diazonium salt intermediate, which rapidly undergoes a nucleophilic aromatic substitution with *N*-(1-naphthyl)ethylenediamine to produce the azo dye.[22] While similar reagents can, and have been, be used,[22,23] these reagents are commonly regarded as the optimal choices. *N*-(1-Naphthyl)ethylenediamine is the most sensitive, rapid, and pH tolerant of the known potential candidates,[8] and sulfanilamide reacts rapidly with *N*-(1-

Received: February 14, 2020
Accepted: March 12, 2020
Published: March 12, 2020

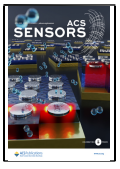

https://dx.doi.org/10.1021/acssensors.0c00291
ACS Sens. 2020, 5, 1207−1215

Scheme 1. Reaction of the Griess Reagents, *N*-(1-Naphthyl)ethylenediamine and Sulfanilamide, with Nitrite to Form an Azo Dye, Which Is Commonly Used for Nitrite Detection

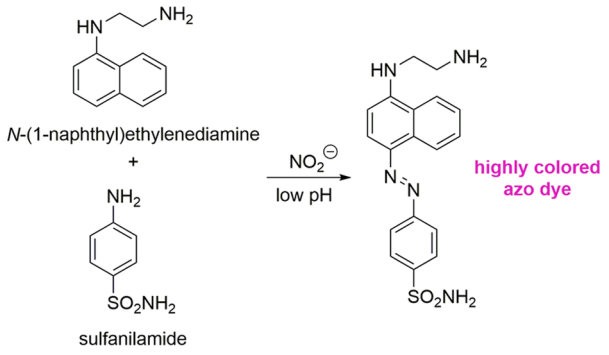

naphthyl)ethylenediamine and nitrite to produce a stable colored product within seconds.[23] Therefore, these compounds were used for this study.

Several paper-based devices using the Griess method for nitrite detection have been reported in recent literature.[13,15,18] While these have allowed for NO_2^- detection limits as low as 1.0 μM (46 ppb),[15] 0.65 μM (30 ppb),[13] and 0.86 μM,[24] with testing ranges of 10−150, 1.1−220, and 0.88−12 μM, respectively, these concentrations are still too high for environmental monitoring applications. In addition, most of these devices suffer from poor stability, with the Griess reagents degrading on the order of several days, which further limits the long-term system performance.[15,18] Furthermore, these devices as well as commercially available devices utilize free (i.e., unaffixed) Griess reagents, allowing both the reagents and the colored azo product to be diluted by sample flow and runoff.

Reported herein is the development and implementation of a *N*-(1-naphthyl)ethylenediamine-cellulose material into a paper-based nitrite sensor, shown in Figure 1. This device was designed to improve the method sensitivity by affixing the colored product to a defined location on the device and has enabled the ultrasensitive (sub-micromolar) detection of nitrite in aqueous media.

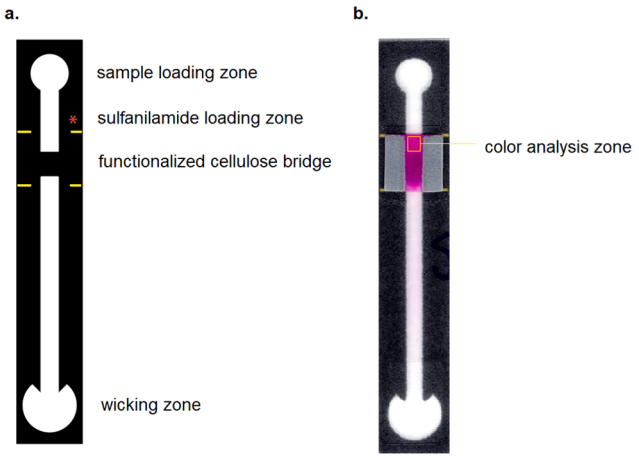

Figure 1. (a) Adobe Illustrator generated image of the paper-based device. (b) Scanned image of the device with immobilized indicator after exposure to 150 μM nitrite.

EXPERIMENTAL SECTION

Cellulose Functionalization. The Whatman 602h paper substrate was patterned using a wax printer to create a 2.5 mm × 10 mm^2 hydrophilic lane with 3.75 mm × 10 mm^2 hydrophobic barriers on each side. The wax was melted in a 120 °C oven for 2.5 min. To an Erlenmeyer flask bearing a 24/40 ground glass joint and a stirbar was added the paper substrate, *N*-(1-naphthyl)-ethylenediamine·HCl (0.833 w/w% to cellulose), and acetonitrile (to create a 0.022 M solution of *N*-(1-naphthyl)ethylenediamine). This solution was sonicated for 30 min, then 1,8-diazabicyclo[5.4.0]-undec-7-ene (DBU) (3.0 equiv relative to *N*-(1-naphthyl)-ethylenediamine) was added and the solution was heated to 55 °C for 30 min with gentle stirring at 100 rpm. Epichlorohydrin (ECH) (3.3 equiv relative to *N*-(1-naphthyl)ethylenediamine) was then added, a condenser was attached to the Erlenmeyer flask, and the solution was heated to 55 °C for 72 h. The solution was then cooled to room temperature. The supernatant was decanted, and the functionalized paper was washed thoroughly with acetonitrile (2×), distilled water (2×), 1.0 M HCl (2×, 1 min each), and distilled water (4×). The functionalized paper was collected on a Buchner funnel and vacuum was pulled for 30 min. The paper was further dried in an oven at 50 °C for 30 min and then stored in a capped vial away from direct light.

Fluorescence Calibration Curves. To each of the 84 wells of a 96-well plate was added a circular 6 mm piece of Whatman #1 (or Whatman 602h) filter paper. A solution of 0.52 mg of *N*-(1-naphthyl)ethylenediamine in 1.0 mL of ultrapure water was created and then diluted by serial dilution to concentrations of 0.48, 0.44, 0.40, 0.36, 0.32, 0.28, 0.24, 0.20, 0.16, 0.12, 0.08, 0.064, 0.048, 0.032, 0.016, 0.008, 0.004, and 0.002 mg/mL. To the first four wells was added 5 μL of the 0.52 mg/mL solution, to the second four wells was added 5 μL of the 0.48 mg/mL solution, etc., until all wells were filled, with 5 μL of ultrapure water added to the last four wells. The solutions were allowed to dry for 2 h in the dark and then the fluorescence of each well was analyzed using a BioTek Instruments Synergy H1 microplate reader with the following parameters: excitation of 300 nm, emission of 340−575 nm, gain of 45; data interval of 1 nm, read height of 10.68 mm. The fluorescence integration of each spectrum (fluorescence intensity by wavenumber) was obtained using OriginPro2018 and the average and standard deviation values were obtained. OriginPro2018 nonlinear curve fitting was applied to the data and an exponential curve fitting was obtained. The values for the degree of functionalization were obtained using Excel Solver and the obtained equation.

Device Construction. All devices were printed in triplicate for an easier comparison of identical measurements (dimensions are shown in Figure S2) and melted in a 120 °C oven for 2.5 min. Self-adhesive no-heat laminate cut to the dimensions shown in Figure S2 was placed on the front of the device so that the sample loading zones and wicking zones were left uncovered. The device was flipped over and 5 μL of a 50 mM sulfanilamide solution (8.6 mg sulfanilamide per 1.0 mL of 1.0 M hydrochloric acid) was deposited in the hydrophilic channel at the location indicated in Figure 1. The solution was allowed to dry for 30 min and then immobilized *N*-(1-naphthyl)-ethylenediamine "bridge" was adhered to the location indicated by yellow reference lines in Figure 1 using double-sided tape. An uncut piece of self-adhering no-heat laminate and pressure lamination was used to seal the device.

Nitrite Detection. *Using Paper Sensors.* Fifty microliters of nitrite sample solution was applied to the paper-based sensors, followed by a 10 min incubation time. Device images were collected using an EPSON v19 Perfection flatbed scanner (with an interleaving absorbent sheet of paper placed on top of the devices to avoid scanner contamination) and analyzed using ImageJ to obtain Normalized Green Values (NGV). Alternatively, naked-eye detection could be achieved within 2 min.

Using Ion Chromatography. A Lachat QuikChem 8500 flow injection analysis system was used for nitrite detection using

https://dx.doi.org/10.1021/acssensors.0c00291
ACS Sens. 2020, 5, 1207−1215

QuikChem Method 31-107-05-1-A provided by Lachat Instruments. The samples were filtered through 0.2 μm filters prior to testing.

Limits of Detection and Quantitation. Nitrite solutions with concentrations of 100, 82.5, 70, 65, 60, 55, 50, 45, 40, 35, 30, 25, 20, 15, 10, 5, 3.5, 2.0, 1.5, 1.25, 1.0, 0.75, 0.50, 0.25, 0.10, and 0.05 μM were created by serial dilution from a 14.5 mM sodium nitrite (1 mg/mL) solution in the appropriate media (i.e., ultrapure water, freshwater, or Sargasso seawater). OriginPro 2018 nonlinear or linear curve-fitting model was applied to the data until the highest R^2 value was obtained. Excel Solver was used with the equation obtained from the curve fitting to find the concentration of nitrite (x) corresponding to the calculated signal responses (y) for the limit of detection (LOD) and the limit of quantitation (LOQ). y_{LOD} and y_{LOQ} were calculated using the equations: $y_{LOD} = \overline{y}_B + 3\sigma_B$ and $y_{LOQ} = \overline{y}_B + 10\sigma_B$, where $\overline{y}_B$ is the average signal response of the blank measurement and σ_B is the standard deviation of the blank measurement.[25] Three replicates were conducted for each measurement in ultrapure water and six replicates were conducted for each measurement in synthetic freshwater or Sargasso seawater.

Interference Studies. *Salinity.* Samples of nitrite in the solutions of known salinity were created using Coral Pro Sea Salt. Concentrations of 4.0, 3.5, 3.3, 3.0, 2.5, 1.5, and 0.5% salt were then created by serial dilution from a solution with a salinity of 4.5% (45 ppt), which was created by dissolving 0.491 g of salt mix in 10 mL of a solution of 50 μM nitrite in ultrapure water. The samples of 15 and 7.5% were created by serial dilution from a solution with a salinity of 30% (300 ppt) that was created by dissolving 3.71 g of salt mix in 10 mL of a solution of 50 μM nitrite in ultrapure water.

Temperature and Relative Humidity. The temperature was controlled in a Boekel Scientific digital incubator and the relative humidity (RH) was adjusted using desiccant and water as needed to achieve the desired relative humidity. Temperature and relative humidity were monitored using an AcuRite digital humidity and temperature comfort monitor. The devices were prepared using the optimal paper functionalization and device construction procedures. The devices were then acclimated under the desired testing conditions for 30 min and then 50 μL of sample solution (0, 10, 50, or 100 μM nitrite in ultrapure water) was added, and the devices were allowed to further incubate in the testing conditions for 10 min to allow the readout to develop.

Turbidity. Suspensions of 1, 5, and 10 mg/mL of Kaolin clay[26] in the nitrite sample solution (0, 10, 50, and 100 μM) were created and then allowed to stir vigorously overnight.

Chemical. One hundred micromolar solutions of potential ion interferents were created and then combined with equal amounts of 100 μM sodium nitrite solution in ultrapure water to create solutions of 50 μM nitrite + 50 μM interferent.

Longevity Studies. The prepared devices were stored under one of five conditions: (1) in the open air with ambient lighting and temperature, (2) vacuum-sealed with ambient lighting and temperature, (3) vacuum-sealed in darkness with ambient temperature, (4) vacuum-sealed in darkness at $\leq$4 °C, and (5) vacuum-sealed in darkness at $\leq$−20 °C. The devices stored under conditions 4 or 5 were allowed to acclimate for 2 h before they were removed from the vacuum packaging and used. Vacuum sealing was achieved using a White Dolphin automatic vacuum sealer model number 02G and Nutri-Lock vacuum sealer bags.

RESULTS AND DISCUSSION

Paper-Based Device Design. To achieve a significant increase in sensitivity toward nitrite detection using a paper-based device, we envisioned a device that would allow a large sample volume to interact with the detection zone without the dilution of the indicators or colored product due to the solution flow or runoff. This was accomplished by the immobilization of a single indicator, and thus the colored product, at the detection zone. The difference between mobile and immobile indicators, shown in Figure 2, is the diffuse color

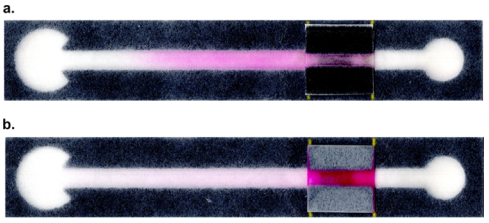

Figure 2. Comparison of (a) mobile and (b) immobile *N*-(1-naphthyl)ethylenediamine when treated with 150 μM nitrite.

obtained via the transportation of the colored product throughout the length of the device with the mobile chromophore (Figure 2a) in contrast to the darker, localized coloration of the detection zone with the immobile indicator (Figure 2b). Of the two reactive components necessary for nitrite detection, *N*-(1-naphthyl)ethylenediamine was chosen as the molecule to graft to the cellulose because sulfanilamide and nitrite react first to form a diazonium salt[22] before the reaction with *N*-(1-naphthyl)ethylenediamine can occur. While immobilization of both indicators was considered, additional difficulties would arise from such a design, including those from the protection and deprotection of sulfanilamide required for functionalization. Additionally, the distance between potential functionalization sites and reduced flexibility of species upon binding may lead to the inhibition of reaction between the two bound indicators.

The optimized paper-based device, shown in expanded view in Figure 3, was designed with a sulfanilamide/nitrite sample

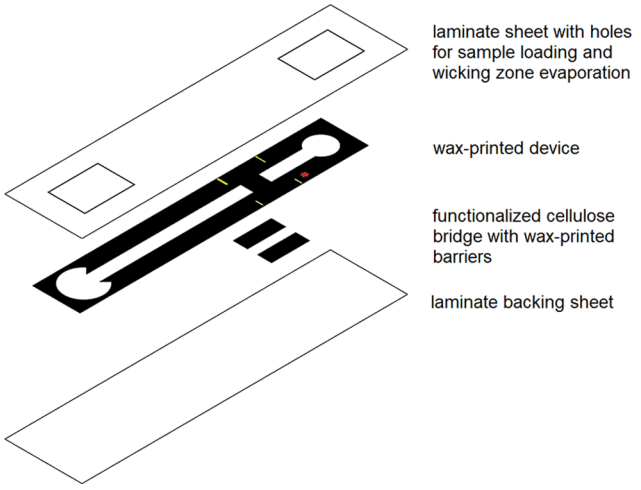

Figure 3. Expanded view of the layers present in the optimized device architecture.

mixing zone, followed by a *N*-(1-naphthyl)ethylenediamine-functionalized cellulose bridge detection zone, and ending with an extended wicking channel, which optimizes the sample flow over and interaction with the functionalized detection zone. Details of the device architecture optimization studies can be found in the Supporting Information.

Functionalization of Cellulose. Immobilization of small molecules to cellulose has been previously achieved using a variety of methods,[27−34] although only one example of functionalized cellulose for nitrite detection has been reported, using 1-naphthylamine rather than *N*-(1-naphthyl)-ethylenediamine.[35] Drawbacks to this published method include that the functionalization procedures were chemically

https://dx.doi.org/10.1021/acssensors.0c00291
ACS Sens. 2020, 5, 1207−1215

detrimental to cellulose, the indicator (1-naphthylamine) is carcinogenic,[8] and that the sub-micromolar detection was only achieved via absorbance spectroscopy or by treating the paper repeatedly with the sample solution. A more favorable approach for the immobilization of *N*-(1-naphthyl)-ethylenediamine is the use of the linker epichlorohydrin, which has been reported in the grafting of small molecules[36] and macrocycles[37,38] to cellulose, typically using aqueous sodium hydroxide conditions.[37,38] However, under these conditions, epichlorohydrin is known to undergo hydrolysis[39−42] or form other unfavorable side products[43] due to the presence of a strongly nucleophilic base and a nucleophilic solvent, which limits the efficacy of functionalization. Additionally, *N*-(1-naphthyl)ethylenediamine is moisture sensitive and poorly water-soluble. Thus, new, more mild conditions were investigated using inert organic solvents and non-nucleophilic bases.

Optimized conditions for the grafting of cellulose with *N*-(1-naphthyl)ethylenediamine are shown in Scheme 2, using

Scheme 2. Optimized Method for the Functionalization of Cellulose with *N*-(1-Naphthyl)ethylenediamine for Nitrite Detection

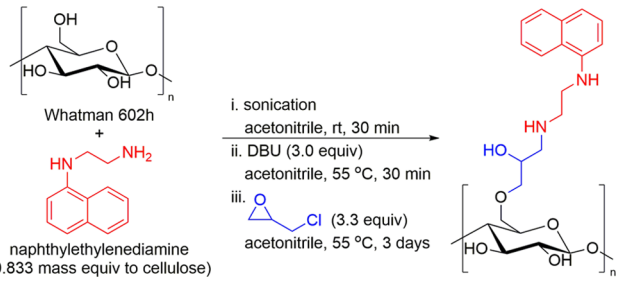

epichlorohydrin as a linker in the presence of 1,8-diazabicyclo[5.4.0]undec-7-ene (DBU) and acetonitrile, with a prefunctionalization sonication[44,45] step designed to provide more sites for grafting by minimally degrading the cellulose substrate.[46−48] These conditions were superior, in terms of *N*-(1-naphthyl)ethylenediamine functionalization density, when compared to aqueous sodium hydroxide conditions[37,40] as indicated by both colorimetric and fluorimetric analyses. While the wax is minimally dissolved in the organic solvent, the hydrophobic barriers were found to remain intact and functional for use in the paper-based device. Detailed reaction optimization studies and procedures for colorimetric and fluorimetric analyses can be found in the Supporting Information.

The functionalization densities of *N*-(1-naphthyl)-ethylenediamine on cellulose under various conditions, summarized in Table 1, were calculated using solid-state fluorescence spectroscopy, for which a calibration curve can be found in Figure 4. Conditions using DBU as a base and acetonitrile as a solvent were 4.8-fold more effective, in terms of functionalization density, than aqueous sodium hydroxide conditions. Further optimization of the DBU/acetonitrile conditions, including the use of sonication and Whatman 602h (condition 4, Table 1), increased the functionalization density to 12.9 times that of the aqueous sodium hydroxide conditions. The small pore size (<2 μm) of Whatman 602h may contribute to the higher functionalization density observed. Corroborating these results, a more intense color

Table 1. Calculated Functionalization Densities[a]

condition	functionalization density (ng/mm^2)
1	6.93 (±2.8)
2	33.3 (±1.5)
3	65.0 (±4.7)
4*	89.1 (±7.6)

[a](1) Whatman #1 (50 mg), *N*-(1-naphthyl)ethylenediamine (NED) (215 mg), epichlorohydrin (ECH) (0.097 mL), 2.0 M NaOH (10 mL), 50 °C for 18 h. (2) Same as (1) but NaOH replaced with DBU (0.25 mL), acetonitrile (10 mL). (3) Whatman #1 (50 mg), NED (42 mg), ECH (0.042 mL), DBU (72 mg), acetonitrile (7.3 mL), 55 °C for 72 h. (4) Conditions shown in Scheme 2. *Calculated using the fluorescence calibration curve for Whatman 602h (Figure S13).

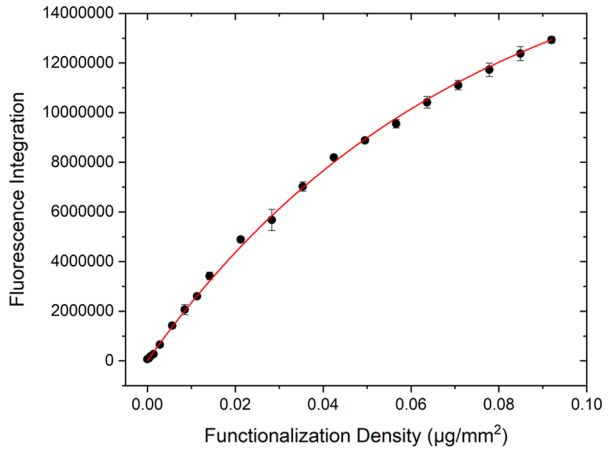

Figure 4. Fluorescence calibration curve for the determination of the functionalization density on Whatman #1. An exponential curve model (red line) with an equation of $y = A^{(-x/t)} + y_0$ was fit to the data where $A = -1.788 \times 10^7$ ($\pm 8.314 \times 10^5$); $t = 0.07176$ (± 0.00495); $y_0 = 1.790 \times 10^7$ ($\pm 8.351 \times 10^5$); and $R^2 = 0.9984$.

change was produced when the optimally functionalized paper was treated with sulfanilamide and nitrite in acidic conditions.

Detection and Quantitation Limits. Concentrations of nitrite in ultrapure water from 0.5 to 50 μM were tested using the sensor. From this, both a calibration curve (Figure 5), for computer-based quantitative detection, and a color readout scale (Figure 5 inset), for qualitative naked-eye detection, were generated. From the former, the limits of detection and quantitation for this method were calculated to be 0.087 and 0.29 μM, respectively.

Detection efficacy was next compared in synthetic freshwater[49] and a real seawater sample from the Sargasso Sea,[50] which differ in both salinity and trace ion content. Calibration curves, using concentrations as low 0.05 μM, in both of these media are shown in Figure 6, and it is clear from the changes in the calibration curve slope that the increased salinity enhances the device readout. Despite this, the limits of detection and quantification are similar to that in ultrapure water (Table 2). The calculated limits of detection and quantitation for the freshwater and saltwater systems are likely more accurate than those of the ultrapure water system, as the testing ranges of the former encompass the calculated values.

Environmental Interference Studies. As the end goal of this sensor development is an onsite application, the robustness of these devices to typical environmental conditions, including temperature, humidity, salinity, and

https://dx.doi.org/10.1021/acssensors.0c00291
ACS Sens. 2020, 5, 1207−1215

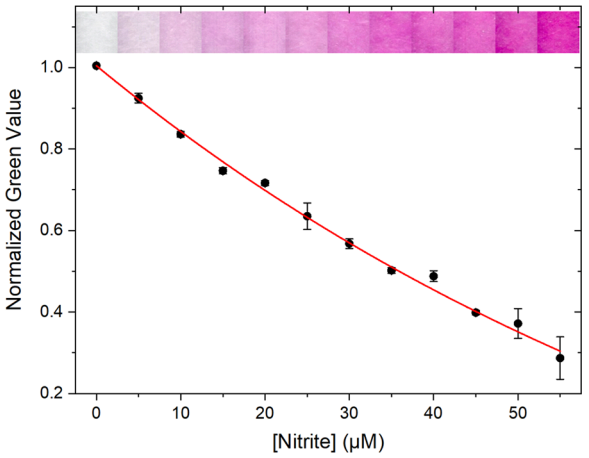

Figure 5. Calibration curve for nitrite response in ultrapure water. The data were fit to an exponential decay curve $y = A^{(-x/t)} + y_0$, where A = 1.519 (±0.2561); t = 88.94 (±18.64); y_0 = −0.5144 (±0.2561); and R^2 = 0.9989. Inset shows a color scale that corresponds to each of the points in the curve.

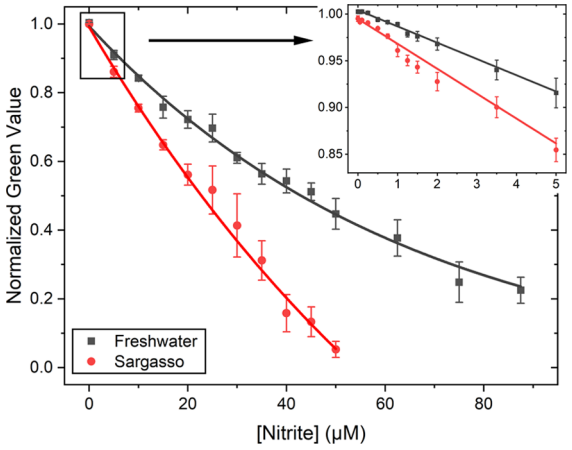

Figure 6. Nitrite calibration curves, in synthetic freshwater (gray) and Sargasso seawater (red) fit to exponential decay curves. Inset shows low nitrite concentrations calibration points (0.05−5 μM).

Table 2. Comparison of Limits of Detection (LODs) and Limits of Quantification (LOQs) Using Different Media

media	LOD (μM)	LOQ (μM)	testing range (μM)
ultrapure water	0.087	0.29	5.0−55
freshwater	0.26	0.69	0.05−50
seawater	0.22	0.89	0.05−85

turbidity, were examined as these have the potential to dramatically impact the device performance.[10]

As indicated by the differences in calibration curve slopes between freshwater and seawater media (vide supra), salinity has a significant influence on sensor readout, a result that has previously been reported with Griess-based colorimetric detection.[51,52] As shown in Figure 7, the sensor readout for 50 μM nitrite in a 0% saline solution matches the readout from the freshwater calibration curve, the upper and lower bounds of which are indicated by the red bar in Figure 7. For 50 μM nitrite solutions in 1.5−4.5%, the sensor readout falls within the standard deviation of the saltwater calibration curve, as shown by the blue bar in Figure 7. This indicates that the saltwater calibration curve can be used to accurately predict the

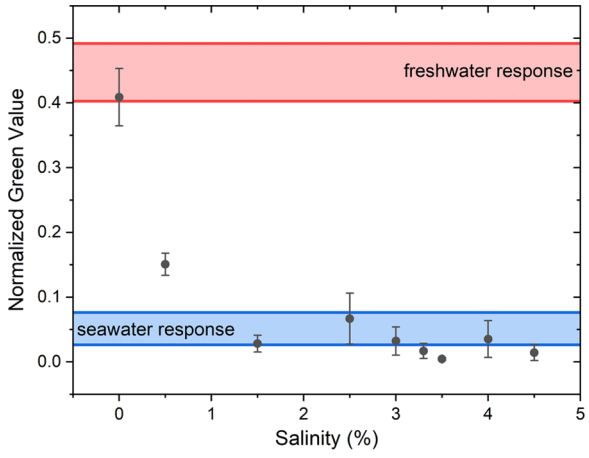

Figure 7. Comparison of sensor readout for samples of 50 μM nitrite (black dots) in various saline solutions. The bars indicate the upper and lower bounds (from average and standard deviation values) for the readout of 50 μM nitrite in Sargasso seawater (blue bars) and synthetic freshwater (red bars).

nitrite concentrations for normal ocean saline (3.0−3.5%)[53] and briny (3.5−7.5%)[54] waters without requiring the measurement of the salinity or additional calculations to account for salinity. Higher salinities, up to 15%, also followed this trend; however, extremely hypersaline water (30%), akin to Dead Sea[55] or Great Salt Lake[56] waters, led to a near-complete degradation of the sensor readout (Figure S32).

Salinity-based readout discrepancies may be explained by two factors: the increase in surface tension and electrostatic potential provided by NaCl leads to changes in the capillary action and flow rate of the system,[57] or the ionic strength of the seawater media might directly affect the equilibrium of the Griess reaction.[51]

The saturation of paper in high-humidity conditions effects not only the amount of sample evaporation but also the speed and rate at which the sample flows through the device channels.[58] Temperature has been previously found to have an effect on the reaction kinetics of the Griess reaction at low (10 °C) and high (40 °C) temperatures.[23] At nitrite concentrations of 50 μM and below, the relative humidity did not affect the device performance between a range of 14−91% (Figure 8a). However, upon examination of 100 μM nitrite, increasing the relative humidity led to an increased device performance (i.e., a lower Normalized Green Value). Temperature had an opposite effect on the device performance, with a temperature of 45 °C leading to a decreased sensor readout at all nitrite concentrations examined (Figure 8b). These interferences are potentially due to changes in device flow rate, with increased humidity leading to less sample evaporation, slower flow rate, and darker sensor readout, while increased temperatures lead to more sample evaporation, faster flow rate, and lighter sensor readout. Thus, for nitrite concentrations of 50 μM or lower, these sensors can be reasonably used at all relative humidities and between temperatures 15 and 35 °C.

Turbid water samples, i.e., those with suspended particulate matter, often require filtration before analytical techniques can be performed, especially when using optical methods,[59] but also when using certain paper-based devices,[18] particularly when highly colored particulate matter may interfere with the sensor readout.[20] However, the filtration ability of the paper

https://dx.doi.org/10.1021/acssensors.0c00291
ACS Sens. 2020, 5, 1207−1215

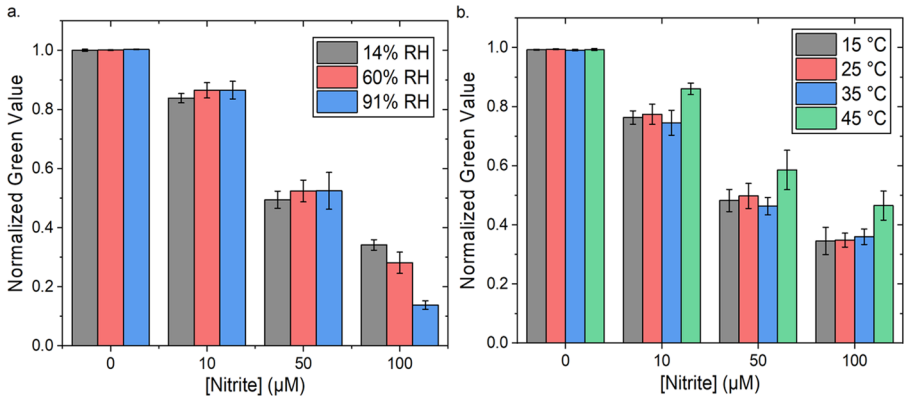

Figure 8. Comparison of sensor readouts, using 0, 10, 50, or 100 μM nitrite solutions, through ranges of (a) relative humidity (RH) and (b) temperature. Bars indicate standard deviation.

substrate used in these devices eliminates the need for prefiltration procedures.[10] This finding was supported by the fact that sensor performance, shown in Figure S33, was unaffected by low, moderate, and high turbidities, which were mimicked using varying amounts of Kaolin clay.[26]

Chemical Interference Studies. A variety of cations and anions were examined for sensor interference, including those that are commonly found in seawater, such as Na^+, K^+, Mg^{2+}, Cl^-, and SO_4^{2-},[60] ions that may be found in trace amounts in seawater, such as F^-, Br^-, NO_3^-, PO_4^{3-}, Co^{2+}, and Zn^{2+},[61,62] or those that have been previously reported to be detrimental to the Griess detection scheme, such as acetate[15] Cu^{2+},[63] S^{2-}, and I^-.[8] Upon examination of nitrite samples with equal concentrations of potential anion interferents, I^-, CO_3^{2-}, $S_2O_3^{2-}$, SO_4^{2-}, and SO_3^{2-} were found to moderately impact the sensor readout (Figure S34). Additionally, the presence of the cations Al^{3+} and Zn^{2+} led to the minimal readout interference at the low concentrations examined (Figure S35).

Real-World Samples. Environmental samples from a variety of locations and containing differing levels of organic matter and suspended solids were successfully analyzed for the presence of nitrite using these devices, and nitrite concentrations were calculated using the appropriate calibration curve. The samples chosen were a home marine aquarium, which many current commercially available nitrite test strips are marketed towards, and the August 2017 Hurricane Harvey floodwaters from Houston, Texas. Only minimal differences between filtered (gray bar, Figure 9) and unfiltered water (red bar, Figure 9) samples from the same source were observed, further supporting the robustness of these devices toward turbidity and large particulate contamination. Confirmation of the quantification accuracy of these measurements was conducted using Lachat ion chromatography (blue bar, Figure 9). While the Lachat quantification matched well with the home marine aquarium, NW Houston, and downtown Houston sensor measurements (all within 0.5 μM), the SE Houston sensor measurements were lower than that of the Lachat quantification by 1.4 μM. Potential sources of this error could be either the paper sensors or the Lachat instrument and may have arisen from the contamination of the water source with the aforementioned interferents or other species during the flooding.

Sensor Longevity. Crucial to the commercialization and usability of such devices is their longevity. Of note, the stability of *N*-(1-naphthyl)ethylenediamine increased upon its grafting to cellulose because the readily oxidized primary amine was

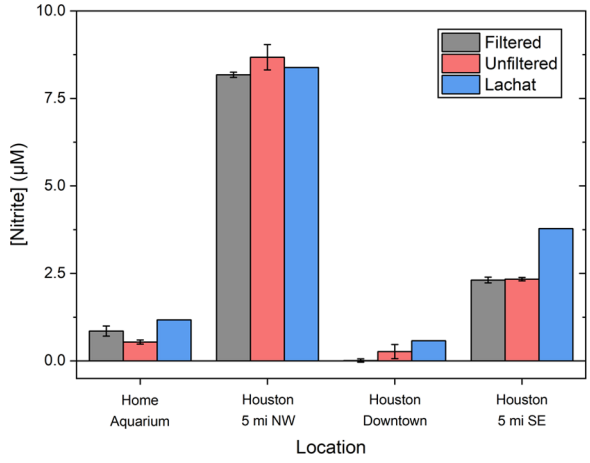

Figure 9. Comparison of the sensor response for filtered (gray) and unfiltered (red) real water samples to Lachat ion chromatography (blue) measurements.

transformed into a much more stable secondary amine (Scheme 2). Fluorescence studies (Figure S37) showed minimal changes in fluorescence over a 110 day period where the functionalized paper was stored in a capped clear vial under ambient temperature and lighting conditions. If *N*-(1-naphthyl)ethylenediamine degradation or oxidation had occurred, a decrease in fluorescence (Figure S38) and discoloration of the functionalized paper would be evident.

Although the covalent linkage of *N*-(1-naphthyl)-ethylenediamine to cellulose effectively stabilizes that component of the Griess reaction (vide supra), the sulfanilamide component remains susceptible to degradation. Under ambient lighting and temperature conditions, the sulfanilamide was stable for less than 24 h. Vacuum sealing of the device and the storage in darkness did little to protect the sulfanilamide from degradation. However, storage at ≤4 and ≤−20 °C extended the device lifetime to 3 and 56 days, respectively (Figure S39). These results are very similar to the component lifetimes reported by Jayawardane et al.[15] and Bhakta et al.[18]

■ CONCLUSIONS

The procedure reported herein allows for the epichlorohydrin-based functionalization of cellulose with *N*-(1-naphthyl)-ethylenediamine using new conditions that are 12.9-fold more effective than when using typical aqueous sodium hydroxide methods.[37,38] The subsequent paper-based device

https://dx.doi.org/10.1021/acssensors.0c00291
ACS Sens. 2020, 5, 1207−1215

implementing the functionalized cellulose allows for detection limits of 0.22 and 0.26 μM for nitrite in Sargasso seawater and synthetic freshwater, respectively, which, to the best of our knowledge, are the lowest values that have been observed using a colorimetric paper-based device for this analyte. The sensor readout is robust in a variety of environmental conditions and was successfully used to analyze several environmental samples without the need for prior sample filtration. In addition, grafting of *N*-(1-naphthyl)ethylenediamine to cellulose improved the stability of *N*-(1-naphthyl)ethylenediamine in the presence of moisture and light.

We are continuing to advance this technology in several ways, including through the enhancement of sulfanilamide stability and device lifetimes, the implementation of a highly efficient nitrate detection scheme, and the application of a smartphone-based color analysis system.

■ ASSOCIATED CONTENT

Supporting Information

The Supporting Information is available free of charge at https://pubs.acs.org/doi/10.1021/acssensors.0c00291.

Details of experimental procedures; optimization studies; colorimetric comparisons; fluorimetric comparisons; and detailed limit of detection calculations (PDF)

■ AUTHOR INFORMATION

Corresponding Author

Mindy Levine − *Department of Chemistry, University of Rhode Island, Kingston, Rhode Island 02881, United States;* orcid.org/0000-0003-4847-7791; Email: mindyl@ariel.ac.il

Authors

Teresa L. Mako − *Department of Chemistry, University of Rhode Island, Kingston, Rhode Island 02881, United States*

Adelaide M. Levenson − *Department of Chemistry, University of Rhode Island, Kingston, Rhode Island 02881, United States*

Complete contact information is available at: https://pubs.acs.org/10.1021/acssensors.0c00291

Author Contributions

All authors have given approval to the final version of the manuscript.

Funding

This research was supported by the National Science Foundation under EPSCoR Cooperative Agreement #OIA-1655221.

Notes

The authors declare no competing financial interest.

■ ACKNOWLEDGMENTS

We would like to thank the following individuals for valuable discussion and feedback about the research described herein: Dr. Brenton DeBoef, Dr. Jason Dwyer, Dr. Charlie Mace, and the Mace research group at Tufts University, especially Dr. Syrena Fernandes. We would also like to thank Dawn Outram, in conjunction with the Marine Science Research Facility, for conducting Lachat Ion Chromatography measurements, Dr. Bethany Jenkins at the University of Rhode Island and her group members for providing the water sample from the Sargasso Sea, Christopher Seveney and Lauren Seveney for providing the Houston floodwater samples, and Red Sea for providing an ICP−MS analysis of the Coral Pro Salt used for mixing synthetic seawater (Figure S1).

■ REFERENCES

(1) Ward, M. H.; Jones, R. R.; Brender, J. D.; de Kok, T. M.; Weyer, pJ.; Nolan, B. T.; Villanueva, C. M.; van Breda, S. G. Drinking Water Nitrate and Human Health: An Updated Review. *Int. J. Environ. Res. Public Health* **2018**, *15*, 1557/1−1557/31.

(2) Jensen, F. B. Nitrite Disrupts Multiple Physiological Functions in Aquatic Animals. *Comp. Biochem. Physiol., Part A: Mol. Integr. Physiol.* **2003**, *135*, 9−24.

(3) Rios-Del Toro, E. E.; Cervantes, F. J. Anaerobic Ammonium Oxidation in Marine Environments: Contribution to Biogeochemical Cycles and Biotechnological Developments for Wastewater Treatment. *Rev. Environ. Sci. Biotechnol.* **2019**, *18*, 11−27.

(4) Ko, Y. H.; Lee, K.; Takahashi, T.; Kari, D. M.; Kang, S.-H.; Lee, E. Carbon-Based Estimate of Nitrogen Fixation-Derived Net Community Production in N-Depleted Ocean Gyres. *Global Biogeochem. Cycles* **2018**, *32*, 1241−1252.

(5) Goudarzi, S.; Jozi, S. A.; Monavari, S. M.; Karbasi, A.; Hasani, A. H. Assessment of Groundwater Vulnerability to Nitrate Pollution caused by Agricultural Practices. *Water Qual. Res. J.* **2017**, *52*, 64−77.

(6) Sajil Kumar, P. J.; Jegathambal, P.; James, E. J. Chemometric Evaluation of Nitrate Contamination in the Groundwater of a Hard Rock area in Dharapuram, South India. *Appl. Water Sci.* **2014**, *4*, 397−405.

(7) Wakida, F. T.; Lerner, D. N. Non-Agricultural Sources of Groundwater Nitrate: A Review and Case Study. *Water Res.* **2005**, *39*, 3−16.

(8) Wang, Q.-H.; Yu, L.-J.; Liu, Y.; Lin, L.; Lu, R.-g.; Zhu, L.-p.; He, L.; Lu, Z.-L. Methods for the Detection and Determination of Nitrite and Nitrate: A Review. *Talanta* **2017**, *165*, 709−720.

(9) Moorcroft, M. J.; Davis, J.; Compton, R. G. Detection and Determination of Nitrate and Nitrite: A Review. *Talanta* **2001**, *54*, 785−803.

(10) Fernandes, S. C.; Walz, J. A.; Wilson, D. J.; Brooks, J. C.; Mace, C. R. Beyond Wicking: Expanding the Role of Patterned Paper as the Foundation for an Analytical Platform. *Anal. Chem.* **2017**, *89*, 5654−5664.

(11) Martinez, A. W.; Phillips, S. T.; Butte, M. J.; Whitesides, G. M. Patterned Paper as a Platform for Inexpensive, Low-Volume, Portable Bioassays. *Angew. Chem., Int. Ed.* **2007**, *46*, 1318−1320.

(12) Buser, J. R.; Byrnes, S. A.; Anderson, C. E.; Howell, A. J.; Kauffman, P. C.; Bishop, J. D.; Wheeler, M. H.; Kumar, S.; Yager, P. Understanding Partial Saturation in Paper Microfluidics Enables Alternative Device Architectures. *Anal. Methods* **2019**, *11*, 336−345.

(13) Vidal, E.; Lorenzetti, A. S.; Lista, A. G.; Domini, C. E. Micropaper-Based Analytical Device (μPAD) for the Simultaneous Determination of Nitrite and Fluoride using a Smartphone. *Microchem. J.* **2018**, *143*, 467−473.

(14) Fàbrega, C.; Fernández, L.; Monereo, O.; Pons-Balagué, A.; Xuriguera, E.; Casals, O.; Waag, A.; Prades, J. D. Highly Specific and Wide Range NO2 Sensor with Color Readout. *ACS Sens.* **2017**, *2*, 1612−1618.

(15) Jayawardane, B. M.; Wei, S.; McKelvie, I. D.; Kolev, S. D. Microfluidic Paper-Based Analytical Device for the Determination of Nitrite and Nitrate. *Anal. Chem.* **2014**, *86*, 7274−7279.

(16) Cardoso, T. M. G.; Garcia, P. T.; Coltro, W. K. T. Colorimetric Detection of Nitrite in Clinical, Food, and Environmental Samples using Microfluidic Devices Stamped in Paper Platforms. *Anal. Methods* **2015**, *7*, 7311−7317.

(17) Jiang, Y.; Hao, Z.; He, Q.; Chen, H. A Simple Method for Fabrication of Microfluidic Paper-Based Analytical Devices and On-Device Flow Control with a Portable Corona Generator. *RSC Adv.* **2016**, *6*, 2888−2894.

(18) Bhakta, S. A.; Borba, R.; Taba, M., Jr.; Garcia, C. D.; Carrilho, E. Determination of Nitrite in Saliva Using Microfluidic Paper-Based Analytical Devices. *Anal. Chim. Acta* **2014**, *809*, 117−122.

(19) Tsikas, D. Analysis of Nitrite and Nitrate in Biological Fluids by Assays Based on the Griess Reaction: Appraisal of the Griess Reaction in the L-Arginine/Nitric Oxide Area of Research. *J. Chromatogr. B* **2007**, *851*, 51−70.
(20) Nesterenko, E. P.; Murphy, B.; Murray, E.; Moore, B.; Diamond, D. Solid-Phase Test Reagent for Determination of Nitrate and Nitrite. *Anal. Methods* **2016**, *8*, 6520−6528.
(21) Sieben, V. J.; Floquent, C. F. A.; Ogilvie, I. R. G.; Mowlem, M. C.; Morgan, H. Microfluidic Colourimetric Chemical Analysis System: Application to Nitrite Detection. *Anal. Methods* **2010**, *2*, 484−491.
(22) Váradi, L.; Breedon, M.; Chen, F. F.; Trinchi, A.; Cole, I. S.; Wei, G. Evaluation of Novel Griess-Reagent Candidates for Nitrite Sensing in Aqueous Media Identified via Molecular Fingerprint Searching. *RSC Adv.* **2019**, *9*, 3994.
(23) Fox, J. B., Jr. Kinetics and Mechanisms of the Griess Reaction. *Anal. Chem.* **1979**, *51*, 1493−1502.
(24) Zhang, X.-X.; Song, Y.-Z.; Fang, F.; Wu, Z.-Y. Sensitive Paper-Based Analytical Device for Fast Colorimetric Detection of Nitrite with Smartphone. *Anal. Bioanal. Chem.* **2018**, *410*, 2665−2669.
(25) Belter, M.; Sajnóg, A.; Barałkiewicz, D. Over a Century of Detection and Quantification Capabilities in Analytical Chemistry − Historical Overview and Trends. *Talanta* **2014**, *129*, 606−616.
(26) Christy, S. S. J. E.; Balraj, A.; Ramalingam, A.; Jararaman, D. Potential Applications of Ionic Liquids (IL) for the Treatment of Synthetic Turbid Water (STW). *J. Mol. Liq.* **2018**, *256*, 121−126.
(27) Klemm, D.; Heublein, B.; Fink, H.-P.; Bohn, A. Cellulose: Facinating Biopolymer and Sustainable Raw Material. *Angew. Chem., Int. Ed.* **2005**, *44*, 3358−3393.
(28) O'Connell, D. W.; Birkinshaw, C.; O'Dwyer, T. F. Heavy Metal Adsorbents Prepared from the Modification of Cellulose: A Review. *Bioresour. Technol.* **2008**, *99*, 6709−6724.
(29) Nyström, D.; Lindqvist, J.; Östmark, E.; Antoni, P.; Carlmark, A.; Hult, A.; Malmström, E. Syperhydrophobic and Self-Cleaning Bio-Fiber Surfaces via ATRP and Subsequent Postfunctionalization. *ACS Appl. Mater. Interfaces* **2009**, *1*, 816−823.
(30) Boufi, S.; Rei Vilar, M.; Parra, V.; Ferraria, A. M.; Botelho do Rego, A. M. Grafting of Porphyrins on Cellulose Nanometric Films. *Langmuir* **2008**, *24*, 7309−7315.
(31) Navarro, R. R.; Sumi, K.; Fujii, N.; Matsumura, M. Mercury Removal from Wastewater using Porous Cellulose Carrier Modified with Polyethyleneimine. *Water Res.* **1996**, *30*, 2488−2494.
(32) Aloulou, F.; Boufi, S.; Labidi, J. Modified Cellulose Fibres for Adsorption of Organic Compound in Aqueous Solution. *Sep. Purif. Technol.* **2006**, *52*, 332−342.
(33) Martini, R.; Serrano, L.; Barbosa, S.; Labidi, J. Antifungal Cellulose by Capsaicin Grafting. *Cellulose* **2014**, *21*, 1909−1919.
(34) Castro, D. O.; Tabary, N.; Martel, B.; Gandini, A.; Belgacem, N.; Bras, J. Effect of Different Carboxylic Acids in Cyclodextrin Functionalization of Cellulose Nanocrystals for Prolonged Release of Carvacrol. *Mater. Sci. Eng., C* **2016**, *69*, 1018−1025.
(35) Amelin, V. G.; Kolodkin, I. S. Cellulose Paper with Chemically Immobilized 1-Naphthylamine for the Rapid Determination of Nitrite, Nitrate, and Aromatic Amines. *J. Anal. Chem.* **2001**, *56*, 182−187.
(36) Beyki, M. H.; Ghasemi, M. H. Quaternized γ-Fe_2O_3@Cellulose Ionomer: An Efficient Recyclable Catalyst for Michael-Type Addition Reaction. *Int. J. Biol. Macromol.* **2018**, *113*, 711−718.
(37) Zhao, Q.; Wang, S.; Cheng, X.; Yam, R. C. M.; Kong, D.; Li, R. K. Y. Surface Modification of Cellulose Fiber via Supramolecular Assembly of Biodegradable Polyesters by the Aid of Host-Guest Inclusion Complexation. *Biomacromolecules* **2010**, *11*, 1364−1369.
(38) Zhang, F.; Wu, W.; Sharma, S.; Tong, G.; Deng, Y. Synthesis of Cyclodextrin-Functionalized Cellulose Nanofibril Aerogel as a Highly Effective Adsorbent for Phenol Pollutant Removal. *BioResources* **2015**, *10*, 7555−7568.
(39) Yang, X.; Liu, L. Synthesis and Characterization of Novel Polyglycerol Hydrogels Containing L-Lactic Acid Groups as Pendant Acidic Substituents: pH-Responsive Polyglycerol-Based Hydrogels. *J. Appl. Polym. Sci.* **2009**, *112*, 3209−3216.
(40) Semenova, M. V.; Mezhuev, Y. O.; Osadchenko, S. V.; Shtil'man, M. I. Kinetic Features of the Reaction of Polyvinyl Alcohol with Epichlorohydrin in an Alkaline Medium. *Russ. J. Gen. Chem.* **2017**, *87*, 1047−1052.
(41) Lu, Y.; Wang, R.; Zhang, J.; Jin, Q.; Luo, G. Evaluation of an Improved Epichlorohydrin Synthesis from Dichloropropanol using a Microchemical System. *Chin. J. Chem. Eng.* **2015**, *23*, 1123−1130.
(42) Lu, Y.; Li, T.; Wang, R.; Luo, G. Synthesis of Epichlorohydrin from 1,3-Dichloropropanol using Solid Base. *Chin. J. Chem. Eng.* **2017**, *25*, 301−305.
(43) Yao, Y.; Li, Z.; Qiu, Y.; Bai, J.; Su, J.; Zhang, D.; Jiang, S. Unprecedented Reactions: From Epichlorohydrin to Epoxyglycidyl Substituted Divinyl Ether and its Conversion into Epoxyglycidyl Propargyl Ether. *Sci. Rep.* **2015**, *5*, No. 14231. (1-6)
(44) Udoetok, I. A.; Wilson, L. D.; Headley, J. V. Ultra-Sonication Assisted Cross-Linking of Cellulose Polymers. *Ultrason. Sonochem.* **2018**, *42*, 567−576.
(45) Sethi, J.; Oksman, K.; Illikainen, M.; Sirviö, J. A. Sonication-Assisted Surface Modification Method to Expedite the Water Removal from Cellulose Nanofibers for use in Nanopapers and Paper Making. *Carbohydr. Polym.* **2018**, *197*, 92−99.
(46) Stefanovic, B.; Rosenau, T.; Potthast, A. Effect of Sonochemical Treatments on the Integrity and Oxidation State of Cellulose. *Carbohydr. Polym.* **2013**, *92*, 921−927.
(47) Wong, S.-S.; Kasapis, S.; Tan, Y. M. Bacterial and Plant Cellulose Modification using Ultrasound Irradiation. *Carbohydr. Polym.* **2009**, *77*, 280−287.
(48) Csóka, L.; Lorincz, A.; Winkler, A. Sonochemically Modified Wheat Straw for Pulp and Papermaking to Increase its Economical Performance and Reduce Environmental Issues. *BioResources* **2008**, *3*, 91−97.
(49) *Methods for Measuring the Acute Toxicity of Effluents and Receiving Waters to Freshwater and Marine Organisms*, EPA-821-r-02-012; USEPA Office of Water: Washington, DC, 2002; pp 32−34.
(50) Fawcett, S. E.; Johnson, K. S.; Riser, S. C.; Van Oostende, N.; Sigman, S. M. Low-Nutrient Organic Matter in the Sargasso Sea Thermocline: A Hypothesis for its Role, Identity, and Carbon Cycle Implications. *Mar. Chem.* **2018**, *207*, 108−123.
(51) Ahn, J.-H.; Jo, K. H.; Hahn, J. H. Standard Addition/Adsorption Detection Microfluidic System for Salt Error-Free Nitrite Determination. *Anal. Chim. Acta* **2015**, *886*, 114−122.
(52) Zhang, J.; Ortner, P. B.; Fischer, C. J. *Method 353.4 Determination of Nitrate and Nitrite in Estuarine and Coastal Waters by Gas Segmented Continuous Flow Colorimetric Analysis*, EPA/600/R-15/012; United States Environmental Protection Agency: Washington, DC, 1997.
(53) Du, Y.; Zhang, Y.; Shi, J. Relationship Between Sea Surface Salinity and Ocean Circulation and Climate Change. *Sci. China: Earth Sci.* **2019**, *62*, 771−782.
(54) Choi, S.; Kim, B.; Nayar, K. G.; Yoon, J.; Al-Hammadi, S.; Lienhard, V. J. H.; Han, J.; Al-Anzi, B. Techno-Economic Analysis of Ion Concentration Polarization Desalination for High Salinity Desalination Applications. *Water Res.* **2019**, *155*, 162−174.
(55) Qdais, H. A. Environmental Impacts of the Mega Desalination Project: The Red-Dead Sea Conveyor. *Desalination* **2008**, *220*, 16−23.
(56) Tran, T. T. D.; Park, K.; Smith, A. D. System Scaling Approach and Thermoeconomic Analysis of a Pressure Retarded Osmosis System for Power Production with Hypersaline Draw Solution: A Great Salt Lake Case Study. *Energy* **2017**, *126*, 97−111.
(57) Kuchin, I. V.; Matar, O. K.; Craster, R. V.; Starov, V. M. Modeling the Effect of Surface Forces on the Equilibrium Liquid Profile of a Capillary Meniscus. *Soft Matter* **2014**, *10*, 6024−6037.
(58) Castro, C.; Rosillo, C.; Tsutsui, H. Characterizing Effects of Humidity and Channel Size on Imbibition in Paper-Based Microfluidic Channels. *Microfluid. Nanofluid.* **2017**, *21*, No. 21.

(59) Medina-Sánchez, M.; Cadevall, M.; Ros, J.; Merkoçi, A. Eco-Friendly Electrochemical Lab-on-Paper for Heavy Metal Detection. *Anal. Bioanal. Chem.* **2015**, *407*, 8445−8449.
(60) Voigt, W. What We Know and Still Not Know about Ocean Salts. *Pure Appl. Chem.* **2015**, *87*, 1099−1126.
(61) Wang, R.; Wang, N.; Ye, M.; Zhu, Y. Determination of Low-Level Anions in Seawater by Ion Chromatography with Cycling-Column-Switching. *J. Chromatogr. A* **2012**, *1265*, 186−190.
(62) Gao, Y.; Zhou, C.; Gaulier, C.; Bratkic, A.; Galceran, J.; Puy, J.; Zhang, H.; Leermarkers, M.; Maeyens, W. Labile Trace Metal Concentration Measurements in Marine Environments: From Coastal to Open Ocean. *TrAC, Trends Anal. Chem.* **2019**, *116*, 92−101.
(63) Ellis, P. S.; Shabani, A. M. H.; Gentle, B. S.; McKelvie, I. D. Field Measurement of Nitrate in Marine and Estuarine Waters with a Flow Analysis System utilizing On-Line Zinc Reduction. *Talanta* **2011**, *84*, 98−103.

https://dx.doi.org/10.1021/acssensors.0c00291
ACS Sens. 2020, 5, 1207−1215